

Numerical Simulation of Microwave GaAs MESFETs

Christopher M Snowden

Solid State Materials, Devices and Applications Group  
Department of Electrical and Electronic Engineering  
University of Leeds, Leeds LS2 9JT UK

SUMMARY

A comprehensive physical model is used in a two-dimensional numerical simulation of highly doped gallium arsenide MESFETs. Particular attention is paid to the formulation of the numerical schemes and boundary conditions to ensure accurate modelling. A specially formulated current continuity finite difference equation is used, which produces stable, accurate and efficient solutions, even at carrier levels in excess of  $10^{23} \text{ m}^{-3}$  in GaAs devices. Long simulation times, greater than 300pS, are feasible using this simulation, which makes it suitable for analysing continuous wave r.f. responses in addition to d.c. and transient phenomena.

The simulation has been applied to a variety of device structures, including devices with buffer layers, specified doping profiles and highly doped implants at ohmic contacts. Simulated static characteristics of short gate length MESFETs match measured data very closely. Electron heating effects are accounted for in short gate length devices by implementing a detailed electron temperature model.

The highly efficient physical model has been used in the analysis and design of simple microwave monolithic integrated circuits (MMICs). The MESFET model is embedded in a time domain circuit model from which terminal current and voltage responses are extracted and Fourier analysed. This approach has been used successfully in the large-signal analysis of MESFET microwave oscillator operation.

1. INTRODUCTION

The superiority of gallium arsenide (GaAs) field effect transistors over similar silicon devices at microwave frequencies, has led to them being utilized in many applications. Discrete GaAs FETs have been used in low noise microwave

amplifiers for some time. GaAs MESFETs (metal-semiconductor FETs), have already been incorporated in high speed medium-scale integrated circuits operating at data rates of several gigabits per second. Analogue monolithic microwave integrated circuits (MMICs), are currently being developed for applications such as receiver front-ends, synthesisers and phased-array radar. The rapid advances in MMIC FET technology stretches current CAD and modelling techniques to the limit of their validity, and more accurate, flexible models are required to guarantee the successful realisation of future MMICs which use short gate length GaAs FETs.

A rigorous treatment of the analysis and design of microwave MESFETs and associated circuits requires an accurate device model. Analytical techniques are unsuitable for modelling GaAs devices with small gate geometries and small aspect ratios (ratio of gate length to channel thickness), because it is difficult to model the two-dimensional field and carrier distributions in the active channel. Furthermore, it is difficult to account for the complex nature of the material properties of GaAs in simple analytical models, because they lead to highly non-linear carrier transport equations. Similarly, equivalent circuit models, derived from electrical and microwave measurements, are also unsuitable because they are obtained from measurements made at specific frequencies, signal levels, bias levels and in measurement systems of fixed impedance (usually  $50 \Omega$ ), and cannot intrinsically model the non-linear behaviour of MESFETs, under large-signal conditions.

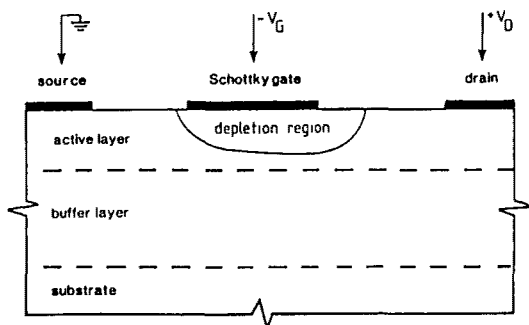


Figure 1  
Planar MESFET Structure

The GaAs MESFET (Schottky barrier gate field effect transistor) is a planar device, with a thin highly doped n-type active layer (usually of the order of  $0.1$  to  $0.25 \mu\text{m}$  thick, with a doping density in excess of  $10^{23}\text{m}^{-3}$ ). The ohmic source and drain contacts are separated by a channel a few microns in length, which includes the gate contact, Figure 1. Gate lengths in the order of  $0.25 \mu\text{m}$  are currently possible.

The material, geometric and carrier transport properties

of short gate length ( $<3 \mu\text{m}$ ) MESFETs are well suited to a physical modelling technique based on a multi-dimensional numerical analysis. In devices with short gate lengths and large gate widths ( $>100 \mu\text{m}$ ), two-dimensional models appear to be adequate. However, for FETs with relatively small gate widths (around 10 to 30  $\mu\text{m}$ ), such as those found in digital circuits, three-dimensional models may be necessary to account for fringing fields [1] [2].

Early numerical simulations for semiconductor devices were based as one-dimensional d.c. simulations, where restrictions on computer memory and time prohibited the consideration of further dimensions. The advent of more powerful computers and a greater understanding of the problem has led to the analysis of more complex devices in two or more dimensions. Two-dimensional FET simulations for d.c. and transient analysis have been described in several papers [3] [4] [5], although less information is available for the a.c. case [6] [7]. The numerical solution becomes more complex for 'multi-valley' semiconductors than for the case of silicon. In particular, it was found that the larger diffusion coefficient of GaAs and InP, compared with Si, can impose severe limitations on the stability of numerical schemes used to model carrier transport.

The numerical simulation must be capable of handling the very high carrier levels ( $>10^{23}\text{m}^{-3}$ ), of the active layer in microwave GaAs MESFETs. Existing simulation schemes, which either dealt with silicon transistors or were formulated for lower doped GaAs devices such as transferred electron devices (TEDs), were generally found to be too inaccurate and lacked numerical stability when they were used to model highly doped GaAs MESFETs. Instabilities which originated at the boundaries of the Schottky barrier depletion region, appeared to be caused by the very high carrier gradients, which in conjunction with the large diffusion coefficient, led to large errors in the solution of the current continuity condition. The current continuity scheme described below overcomes many of the problems and yields stable, accurate solutions for highly doped GaAs devices.

The two-dimensional numerical simulation described in this paper allows the accurate analysis of short gate length MESFET operation by solving a set of electron transport equations for a rigorous physical model. The model takes into account the active layer, buffer layer and substrate as well as modelling non-equilibrium transport conditions. Fast finite-difference schemes are used to implement the numerical solution of the device equations. A novel 'double-iteration' technique was formulated to increase the speed of solution for the Poisson and continuity expressions. Special attention was paid to the boundary conditions in order to maintain accuracy and consistency of the model. In particular, a highly accurate boundary condition for the Schottky Barrier gate contact is

described, which is based on thermionic emission-diffusion theory, and accounts for a wide range of bias conditions. The relatively high efficiency of the device simulation allows large-signal simulations of several hundred picoseconds to be conducted in moderate amounts of computer time. Also, the numerical schemes developed for this simulation only require single precision manipulation by the computer to achieve a high degree of accuracy.

A numerical time domain circuit analysis based on the MES-FET simulation was developed for a lumped element monolithic microwave circuit. Special care was taken in the formulation of the circuit equations, to ensure stability and immunity from small numerical errors in the currents produced in the FET simulation. This simulation technique allows microwave monolithic circuits containing active devices to be accurately modelled, and is particularly useful for large-signal analysis [7] [8].

## 2. THE PHYSICAL DEVICE MODEL

### 2.1. Carrier Transport Modelling

A physical model based on a phenomenological description of the carrier transport equations, derived from the Boltzmann equation, is particularly suitable for device simulations because of the less prohibitive demands on computer facilities compared with either quantum or Monte-Carlo models.

Microwave MESFETs are majority carrier devices, fabricated with n-type GaAs active layers. In the following analysis, minority carriers are neglected and generation and recombination effects are assumed to be negligible. The group of phenomenological equations which describe the carrier transport properties for a multi-valley semiconductor, can be approximated to those of a single-electron gas model [9] [10]. This assumes that the average electron temperature of the electron gases in the upper and lower valleys are the same. Using these assumptions the equations describing the carrier transport process are;

$$\text{Current continuity} \quad \frac{\partial n}{\partial t} = \frac{1}{q} \nabla \cdot \bar{\mathbf{J}}_n \quad (1)$$

where the electron current  $\bar{\mathbf{J}}_n$  is given by

$$\bar{\mathbf{J}}_n = qn\bar{\mathbf{v}} \quad (2)$$

$q$  is the magnitude of the electronic charge,  $n$  is the total electron density (for both valleys),  $\bar{\mathbf{v}}$  is the average electron velocity and  $t$  is time. The momentum conservation equation derived from the Boltzmann equation yields an expression for the average electron velocity of the form,

$$\bar{v} = \mu(\xi)\bar{E} + \frac{k\mu(\xi)}{qn} \nabla(nT_e(\xi)) \quad (3)$$

where  $\mu(\xi)$  is the average electron mobility, which is a function of electron energy  $\xi$ ,  $k$  is Boltzmann's constant and  $T_e(\xi)$  is the electron temperature. The first term on the right hand side of equation (3) represents the average drift velocity of the electron gas. The second term represents the contribution due to diffusion. This expression for the drift and diffusion differs from that usually employed in the "diffusion approximation", where

$$\bar{v} = \mu(E)\bar{E} + \frac{D(E)}{n} \nabla n \quad (4)$$

$$\text{or } \bar{v} = \mu(E)\bar{E} + \frac{1}{n} \nabla(D(E)n) \quad (5)$$

In these commonly used expressions, the mobility  $\mu$  and diffusion coefficient  $D$  are functions of the average electric field  $\bar{E}$ , and not average electron energy  $\xi$  as in equation (3). Secondly, the diffusion term in (3) is not the same as that in either equation (4) or (5). Curtice and Yun [10] have shown, that if the temperature gradients are negligible, then the temperature may be taken out of the gradient term in the diffusion component of equation (3), yielding an expression similar to that of equation (4), where,

$$D(\xi) = \frac{kT_e(\xi)}{q} \mu(\xi) \quad (6)$$

which is the well known Einstein relationship.

The electron temperature  $T_e(\xi)$  is determined from the energy conservation equation,

$$\frac{\partial(n\xi)}{\partial t} + \nabla \cdot (\bar{v}n\xi) \approx qn\bar{v} \cdot \bar{E} - \nabla \cdot (\bar{v}nkT_e) - \frac{n(\xi - \xi_0)}{\tau_e} \quad (7)$$

where  $\tau_e$  is the electron energy relaxation time, which is itself dependent on electron temperature.  $\xi_0$  is the electron energy corresponding to the lattice temperature  $T_0$ . This form of the energy conservation equation assumes a displaced Maxwellian distribution, where higher orders moments of the distribution function disappear. Because of this assumption, heat flow due to the electron gas (the third moment of the distribution function) is not included in equation (7). Blotekjaer points out that this term may be significant in a non-Maxwellian distribution [9]. However, very little information exists on the thermal conductivity of electron gases. The momentum relaxation time is assumed to be constant and it is also assumed for simplicity, that the thermal energy of the electrons is much greater than the kinetic energy, and hence,

$$\xi \approx \frac{3}{2}kT_e \quad (8)$$

As a result of this approximation, the mobility and diffusion coefficients in equation (3) (or (4)) become functions of the electron temperature.

The electric field  $\bar{E}$ , which appears in equations (3) and (7) is obtained from the solution of Poisson's equation, where

$$\nabla^2 \psi = \frac{q}{\epsilon_o \epsilon_r} (N_D - n) \quad (9)$$

Here  $\psi$  is the electrostatic potential,  $N_D$  is the ionized donor density and  $\epsilon_o \epsilon_r$  is the permittivity. The electric field is then obtained from,

$$\bar{E} = - \nabla \psi \quad (10)$$

The total current density  $\bar{J}$  is given by,

$$\bar{J} = \bar{J}_n + \epsilon_o \epsilon_r \frac{d\bar{E}}{dt} \quad (11)$$

Finally, the current  $I$  crossing a plane  $p$  is obtained from the surface integral,

$$I = \int_p \bar{J} ds \quad (12)$$

## 2.2. Material Characteristics

The device equations described previously, require the characteristic relationships between the electron temperature, relaxation time, electric field, and carrier mobility. The steady-state electron temperature dependence on electric field is shown in Figure 2 [11]. A detailed curve fit has been obtained for this characteristic, which is a function of lattice temperature.

Because the electron temperature is a function of applied electric field, the steady-state electron drift velocity can be expressed in terms of a field dependent mobility as

$$\bar{v}(E) = \mu(E)\bar{E} \quad (13)$$

This gives rise to the familiar velocity-field characteristic. A temperature and doping dependent curve fit is shown in figure 3, which is obtained from Freeman and Hobson's relationship [12] and Hilsum's empirical relationship between the low-field mobility  $\mu_o$  and carrier concentration [13],

$$v = \mu(E, T, N_D) = \frac{300\mu_o E}{T} \left[ \frac{1 + \frac{8.5 \times 10^4 E^3}{\mu_o E_o^4 (1 - 5.3 \times 10^{-4} T)}}{(1 + [\frac{E}{E_o}]^4)} \right] \text{ m.s}^{-1}$$

$$E_o = 4 \times 10^5 \text{ V.m}^{-1} \quad (14)$$

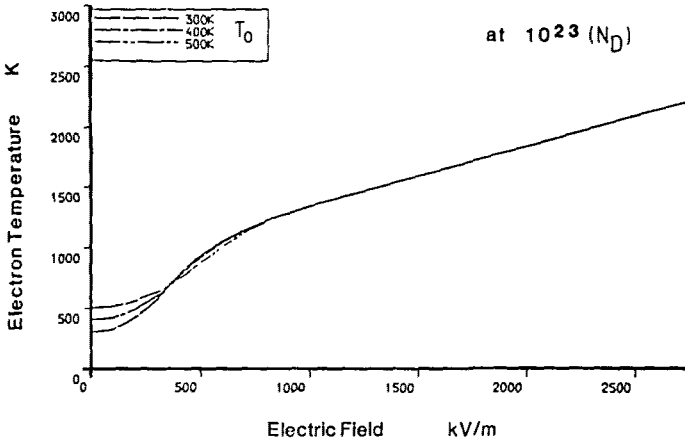


Figure 2

Electron Temperature - Field Characteristic as a function of Lattice Temperature for GaAs

where

$$\mu_o = \frac{0.8}{1 + \sqrt{(N_D/10^{23})}} \quad \text{m}^2\text{V}^{-1}\text{S}^{-1} \quad (15)$$

In the steady state the energy conservation equation reduces to,

$$q\bar{v}(T_e) \cdot E = \frac{3}{2}k \frac{(T_e - T_o)}{\tau_e(T_e)} \quad (16)$$

which together with the velocity field and temperature-field characteristic, allows the energy relaxation time  $\tau_e$  to be determined as a function of electron temperature.

The electron-temperature dependent parameters of GaAs, described above, allow the carrier transport equations to be solved, and account for non-stationary transport conditions within the device. This means that velocity-overshoot can be modelled using this simulation.

### 2.3. Boundary Conditions

The accurate modelling of short gate-length planar MESFET operation has been shown to require at least a two-dimensional solution to the carrier transport equations. A two-dimensional analysis is most conveniently conducted using Cartesian coordinates to describe the rectangular geometry of the planar MESFET model.

Mathematically, the model requires the solution of two quasi-linear, coupled, second-order partial differential equations. These are the elliptic Poisson equation and parabolic continuity equation. The necessary boundary conditions to

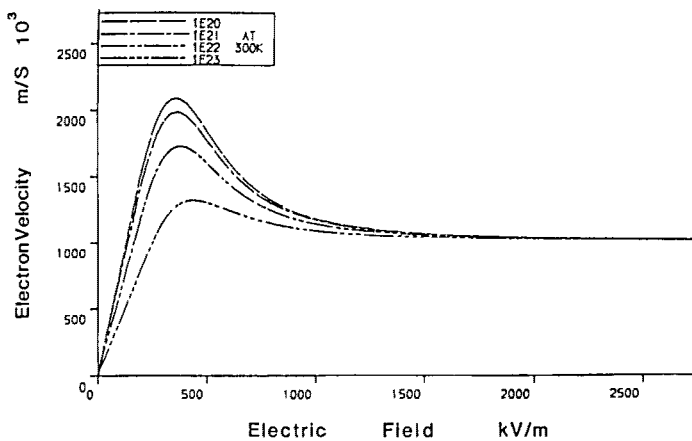
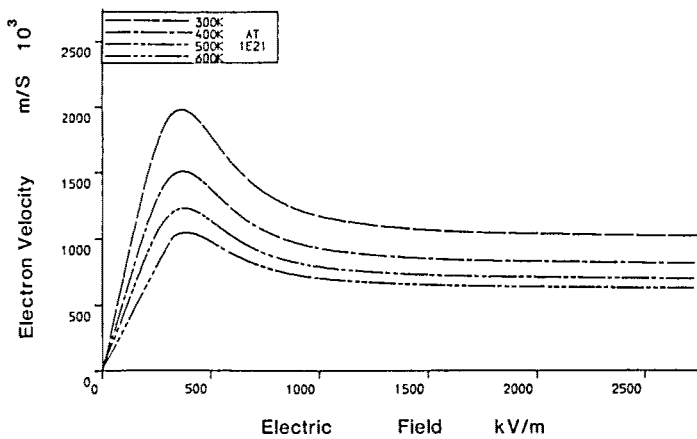


Figure 3  
Temperature and Doping Dependent Velocity-Field  
Characteristics for GaAs

solve this system of equations are two sets of spatial boundary conditions and one initial condition. The surface and contact properties provide the boundary conditions. The presence of current-free boundary regions in addition to ohmic and Schottky contacts leads to mixed boundary conditions.

The absence of current flow through surfaces in the two-dimensional model can be modelled by assuming that the potential and carrier gradients normal to these surfaces are zero, if the surrounding media is assumed to have zero relative permittivity. This leads to the following differential boundary conditions,

$$\frac{\partial \psi}{\partial x}, \frac{\partial n}{\partial x} = 0 \quad \text{for boundaries parallel with the } y \text{ axis} \quad (17)$$

$$\frac{\partial \psi}{\partial y}, \frac{\partial n}{\partial y} = 0 \quad \text{for boundaries parallel with the } x \text{ axis} \quad (18)$$

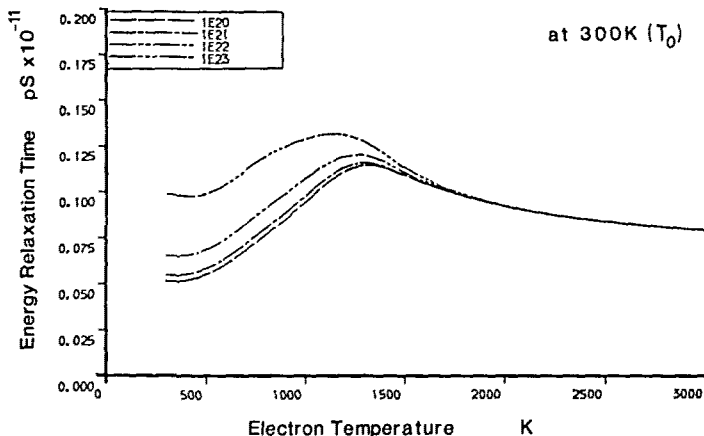


Figure 4  
Energy relaxation time as a function of  
electron temperature for GaAs at  $T_0 = 300$  K

The effects of surface potentials and surface recombination on the top surface of the device are not accounted for here and are currently being investigated.

The contacts are described by Dirichlet boundary conditions where potential  $\psi$  and carrier concentration  $n$  are defined at the contacts. Ohmic contacts are modelled by a uniform applied potential and a constant equilibrium carrier concentration,

$$\psi = v_D, \quad n = N_{CON} \quad \text{at the drain} \quad (19)$$

$$\psi = v_S, \quad n = N_{CON} \quad \text{at the source} \quad (20)$$

where  $v_D$  and  $v_S$  are the instantaneous drain and source voltages and  $N_{CON}$  is the ionized doping density at the contact.  $N_{CON}$  may be used to model  $n^+$  contact regions, by suitable profiling of the doping density.

The operation of the Schottky barrier is accurately modelled using the thermionic emission-diffusion theory which accounts for a wide range of bias conditions [14]. This current injection model was found to produce superior results when compared with the more commonly used 'diffusion model'. The potential difference between the metal and semiconductor bulk gives rise to the flow of electrons into the metal. The depletion region close to the metal interface may be regarded as a sink for electrons, which allows the current density  $J_S$  to be expressed in terms of an effective recombination velocity  $v_r$ ,

$$J_S = q(n_m - n_0)v_r \quad (21)$$

$n_m$  is the electron density close to the contact at the point of maximum potential energy, and  $n_o$  is the quasi-equilibrium density,

$$n_o = N_c \exp \left[ - \frac{q\phi_{bn}}{kT_e} \right] \quad (22)$$

$N_c$  is the effective density of states in the conduction band and  $q\phi_{bn}$  is the barrier height. The effective recombination velocity is given by [14].

$$v_r = \frac{A^*T^2}{qN_c} \quad (23)$$

where  $A^*$  is the effective Richardson constant. Re-arranging equation (21) allows the electron density to be expressed in a form suitable as a boundary condition for the Schottky barrier,

$$n_m = \frac{J_s}{qV_r} + n_o \quad (24)$$

The potential  $\psi_s$  on the semiconductor side of the Schottky barrier is,

$$\psi_s = v_G - \phi_{bn} \quad (25)$$

where  $v_G$  is the instantaneous gate voltage and  $\phi_{bn}$  is the barrier height (0.80 volts for Al, 0.95 volts for Au).

A suitable initial condition for steady state analysis is provided by

$$n(x,y,t=0) = N_D(x,y) \quad (26)$$

For lengthy simulations, or repetitive bias conditions, a considerable amount c.p.u. time can be saved by using steady state solutions for  $n(x,y)$  and  $\psi(x,y)$  obtained previously, as the initial conditions.

### 3. NUMERICAL SCHEMES

The most commonly used numerical techniques for the solution of two-dimensional partial differential equations are finite-difference and finite-element methods, which solve a discretized set of equations across a grid network of points. The finite-element method, provides a flexible means of investigating complex geometries and it has been used successfully to analyse semiconductor devices. However, although it requires fewer nodes than finite-difference schemes, a matrix re-ordering algorithm is necessary to deal with the intricate matrix structure which occurs and this reduces the speed of solution, which is critical in the applications described in this paper. The finite-difference method lends itself easily

to the simple rectangular geometry of the planar MESFET and there is considerable information available on the stability and convergence properties of these schemes [4] [6] [15].

Normalization of the semiconductor device equations has been used by many authors, simplifying the expressions and saving on computer time. This was not used in the MESFET simulation because of the implementation of electron temperature dependent mobility and because of the use of the unconventional form of the diffusion term, which cannot be normalised in the same way as the usual Einstein diffusion relationship. Also, normalisation leads to expressions containing exponentials which take considerably longer to evaluate on computers than simple arithmetic forms of the basic equations. For this reason, solutions to the continuity equation based on solving for the quasi-Fermi level, are also unsuitable in this particular application, despite the high degree of accuracy possible. The additional requirements on computing time, for this type of solution, are too demanding for r.f. simulations, which require many hundreds of time steps, and hence large amounts of c.p.u. time.

The Poisson equation is expressed using the usual 'five-point formula', based on a central-difference expansion, and is solved using an iterative successive-over-relaxation (SOR) scheme to obtain the potential  $\psi$ . The Neumann potential boundary conditions were discretized using Newton's backward-difference formula, where for example in one-dimension, the derivative is expressed as,

$$\frac{d\psi}{dx} = \frac{-3\psi_{n,j} + 4\psi_{n-1,j} - \psi_{n-2,j}}{2\Delta x} + O(\Delta x^2) \quad (27)$$

Here the subscripts  $i, j$  refer to the co-ordinate,  $\Delta x$  and  $\Delta y$  are the space steps. Hence for zero derivative boundary conditions on current-free surfaces the numerical boundary scheme is, for example (in the case of one surface, in the  $x$ -direction),

$$\psi_{1,j} = \frac{1}{3}(4\psi_{2,j} - \psi_{3,j}) \quad (28)$$

The accuracy of this boundary condition is comparable with that of the Poisson scheme, with an error term of order  $(\Delta x^2, \Delta y^2)$ . The use of this boundary condition expression (and the corresponding term for current-free surfaces parallel to the  $x$  axis), leads to a potential coefficient matrix which does not satisfy the diagonal dominance condition required to guarantee convergence. However, despite this irregularity, convergence is normally possible (usually within an average of 4 iterations), although the optimum relaxation factor used in SOR iterative schemes, departs from the theoretical value calculated for diagonally dominant systems (a relaxation factor of 1.8 was used for a 125 x 31 mesh). A particular advantage of this type of boundary condition is that it avoids the need for

external mesh nodes, which, apart from the increase in memory requirements, can lead to strong singularities at the transition between fixed and derivative boundary conditions. The use of the boundary condition in equation (28) was also found to give more accurate results than the more familiar conditions derived from Stirling Polynomials, which require external nodes.

Large-systems of simultaneous equations with sparse coefficient matrices, such as the Poisson scheme, are well suited to iterative solution schemes, where speed and memory requirements compare advantageously with direct methods such as Gaussian Elimination. Another important advantage of iterative methods is that roundoff errors in the solution are limited to those incurred in the final iteration and are normally negligible. Direct elimination methods are subject to significant cumulative roundoff errors and usually require double-precision arithmetic to minimise their effect. Single precision computation was found to be quite adequate in the iterative schemes outlined here. Iterative methods are generally capable of handling complicated (mixed) boundary conditions better than FFT techniques and are relatively simple to program.

The electric field  $\bar{E}$  is obtained in terms of the components  $E_x$  and  $E_y$ , which are expressed in finite difference notation using central-difference schemes. The current continuity equation, which is solved to obtain the carrier distribution  $n$ , is based on a half-point finite-difference expansion in order to avoid significant errors arising in the evaluation of high-order derivative terms (such as  $\nabla^2 n$ ). The value of the function at the half-point is found from the linear average of the function at integer points either side of the half-point. Reiser [9] substitutes  $\bar{v}$  for the drift term in  $\bar{J}$  in equation (1) using drift velocity  $\bar{v}$  rather than  $\mu\bar{E}$ . The difference between the two forms of drift term has been discussed in the literature [16], where it is shown that the expression  $\mu\bar{E}$  more correctly describes the effects of electron heating in GaAs. A further simplification in Reiser's scheme was that the product  $n\bar{v}$  was linearly averaged, rather than linear averages of  $n$  and  $\bar{v}$  being multiplied together. The partially-implicit form of Reiser's scheme, originally developed for silicon MESFETs, was tried in the GaAs MESFET simulation, but was found to be too inaccurate at high carrier levels ( $>10^{23}\text{m}^{-3}$ ). An alternative scheme based on the half-point method, but with more detailed expansions, was developed to model highly doped devices.

Explicit numerical schemes for equation (1) have strong tendencies towards instability and a convergence condition similar to that imposed on the well known gas-diffusion equation applies, where for linear explicit solutions, stability requires [9],

$$\Delta t < \min \left[ \frac{\Delta x^2 \cdot \Delta y^2}{2D(\Delta x^2 + \Delta y^2)}, \frac{2D}{v_{..}^2} \right] \quad (29)$$

where  $\Delta t$  is the time step and  $V_{\infty}$  is the high field saturated velocity. As a result of this condition the time step is severely restricted in the explicit solution, and the accuracy degrades considerably as the time step approaches the limit. A partially implicit scheme similar to the Crank-Nicholson method was applied in an attempt to overcome these limitations. In order to simplify the numerical solution, the continuity scheme is linearised using the following assumption

$$\mu^{k+1} \cdot E^{k+1} = \mu^k E^k \quad (30)$$

The superscript  $k$  refers to the time step. This linearisation means that the continuity scheme has become implicit in carrier density  $n$  and explicit in  $\mu E$ . The continuity scheme thus becomes,

$$\frac{n_{i,j}^{k+1} - n_{i,j}^k}{\Delta t} = \frac{1}{2q} \left[ \nabla \cdot \bar{J}_{i,j} (n^{k+1}, \mu^k E^k) + \nabla \bar{J}_{i,j} (n^k, \mu^k E^k) \right] \quad (31)$$

$$\text{where } \nabla J = \frac{J_{x_{i+1/2,j}} - J_{y_{i-1/2,j}}}{\Delta x} + \frac{J_{y_{i,j+1/2}} - J_{y_{i,j-1/2}}}{\Delta y} \quad (32)$$

The drift term  $\mu^k E^k$  in this equation causes an asymmetric coefficient matrix, which in turn leads to complex eigenvalues in the Jacobi iteration matrix. In iterative schemes using relaxation, the presence of complex eigenvalues necessitates a smaller relaxation factor than in the case of linear elliptic equations. In fact, it was found necessary to use under-relaxation in the solutions for the MESFET (a factor of 0.35 was found optimum for a 125 x 31 mesh). The explicit treatment of the drift term  $\mu E$  in the linearised continuity equation gives rise to non-linear instabilities. These manifest themselves as standing-waves on the required solution for  $n_{i,j}^k$ , when using large time steps, and are amplified rather than damped if the step width is excessive. There are no general results available for the stability analysis of non-linear systems of partial differential equations. The result shown in equation (34) for linear explicit systems appears to provide a sound basis for the choice of the time step  $\Delta t$ , even in partially implicit schemes, where although the time step is still restricted, larger time steps can be used and greater accuracy can be achieved than with explicit schemes.

In order to solve the continuity equation, spatial boundary conditions and an initial condition are required. The Dirichlet boundary conditions discussed earlier were imposed on the ohmic contacts. The Schottky gate contact is modelled using the discretized expression for equation (24).

The current-free surfaces were modelled using a numerical derivative approximation similar to that used in the Poisson solution, based on the Newton backward-difference formula.

Despite the lack of diagonal dominance in the coefficient matrix, which affects the relaxation factor and convergence properties, these mixed boundary conditions were found to produce excellent results with the linearised continuity scheme.

After determining the new carrier distribution from the continuity scheme, the electron temperature  $T_e$  is updated using the energy conservation equation, in an explicit scheme, based on an expansion of the following expression,

$$\frac{\partial T_e}{\partial t} = \frac{2q}{3k} \bar{v} \cdot \bar{E} - \frac{T_e}{n} \frac{\partial n}{\partial t} - \frac{5}{3n} \nabla \cdot (n T_e \bar{v}) - \frac{T_e - T_0}{\tau_e} \quad (33)$$

The total current density  $\bar{J}$  is determined using a finite-difference expansion consistent with the continuity scheme, calculating the total current densities at half-points rather than at mesh points. The displacement current  $\epsilon_0 \epsilon_r d\bar{E}/dt$  is calculated over ten steps (where  $\Delta t < 0.1 \text{ pS}$ ), rather than the usual one, to minimise errors due to small perturbations in the  $\bar{E}$  field caused by numerical errors. The terminal currents are obtained by integrating the current densities across suitable planes in the device.

#### 4. Simulation Details

In order to maintain a strong physical basis for the simulation, the space and time steps must be related to the characteristic distance and time over which actual perturbations in charge occur. The Debye length and differential dielectric relaxation time therefore provide criteria for the choice of stepwidth. In practice this means that for MESFETs with an active channel doping in the order of  $10^{23} \text{ m}^{-3}$ , the space step widths  $\Delta x$  and  $\Delta y$  must be less than  $0.015 \text{ } \mu\text{m}$ , and the time increment is restricted to less than  $0.03 \text{ pS}$ . Values of  $0.015 \text{ } \mu\text{m}$  and  $0.01 \text{ pS}$  respectively, were found to produce highly stable, accurate solutions allowing the Poisson and current continuity schemes to converge to global accuracies of better than  $5 \times 10^{-6} \text{ V}$  and  $10^{-7} \%$  respectively, using single-precision computation.

A mesh of  $125 \times 31$  points was found to be adequate for modelling a  $0.5 \text{ } \mu\text{m}$  gate length MESFET, with a buffer layer and substrate included in the model. The Poisson and continuity difference schemes were implemented using a 'double iteration' scheme, developed especially for this simulation [7]. This technique speeds up the solution of the two sets of equations, by as much as 25%. At a doping level of  $1.5 \times 10^{23} \text{ m}^{-3}$ , one cycle of the simulation was found to take less than  $0.3$  processor seconds on an Amdahl V7 computer. Models based on a simplified set of carrier transport equations, which do not account for electron heating, were found to take even less time (around  $0.25 \text{ S}$ ).

#### 4.1. Device Characteristics

Steady-state d.c. solutions are obtained by running the simulation long enough to allow the initial transients to completely die out. This may take up to 30 pS or more for some bias conditions. Transient and r.f. responses can also be analysed by stimulating the device with appropriate voltage waveforms. In particular, this simulation has been applied to the analysis of simple microwave circuits and for CAD, by embedding the MESFET in a time domain circuit model [7]. This technique is particularly valuable for the large-signal analysis of MESFET circuits.

#### 4.2. MMIC Circuit Modelling

In MMIC circuit modelling applications, the time domain circuit model is stimulated with the required voltage waveforms and the corresponding current response is Fourier analysed. This technique has been applied to the study of MMIC MESFET oscillators, including voltage-controlled oscillators, where the varactor diode has also been modelled using a device simulation. The MESFET oscillator is treated as a negative-conductance circuit, and driven with a signal voltage at a variety of frequencies and amplitudes. The two-terminal current response is Fourier analysed to obtain the amplitude and frequency-dependent admittance seen at the oscillator output. Using this information it is possible to predict the frequency of oscillation, power output, stability and noise properties of a particular circuit configuration [7].

### 5. D.C. MESFET CHARACTERISTICS

A 0.5  $\mu\text{m}$  gate-length GaAs MESFET with an aluminium gate metallization, shown in Figure 5, was characterised using the simulation. The  $I_{DS}/V_{DS}$  curves are shown in Figure 6. The agreement between the simulated characteristics and measurements is very close. The drain and source currents were found to converge to within 1% under steady-state d.c. conditions, illustrating the accuracy of the simulation.

The potential and carrier distributions for the bias condition  $V_{DS} = 5\text{V}$ ,  $V_{GS} = -1\text{V}$  are shown in Figure 7. The carrier distribution clearly indicates the presence of the static dipole region, associated with GaAs MESFETs, which partly penetrates the buffer layer between the gate and drain. The conducting channel beneath the gate depletion region is restricted to a region between the active layer and buffer layer, even at small gate bias voltages. A contour graph of the x component of current density is shown in Figure 8, which clearly shows the significant current path extending in to the buffer layer.

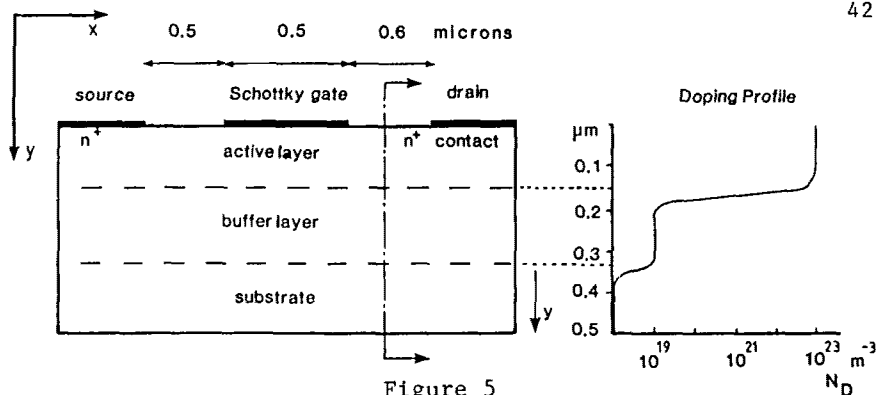


Figure 5  
A 0.5  $\mu\text{m}$  GaAs MESFET with a 300  $\mu\text{m}$  gate width,  
modelled using the simulation

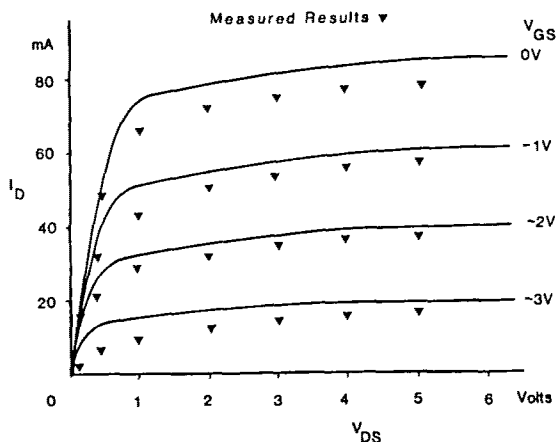


Figure 6  
Simulated d.c. characteristics for  
the 0.5  $\mu\text{m}$  MESFET of Figure 5

## 6. TRANSIENT CHARACTERISTICS

The transient response of the 0.5  $\mu\text{m}$  gate length MESFET is illustrated in Figure 9. A single step function and a square wave pulse have been applied to the gate of the FET, biased with  $V_{DS} = 5\text{V}$ . These responses clearly illustrate the switching behaviour of this type of GaAs FET. The step change in gate potential initially causes a sharp peak due to velocity-overshoot, followed by a large displacement current which dominates the conduction process. After a few picoseconds the remaining transient response is attributable to the carrier transport process. The total decay time for  $i_D$  to drop to 10% of the response is usually in the order of 10 ps, which gives a measure of the time constant associated with the gate capacitance.

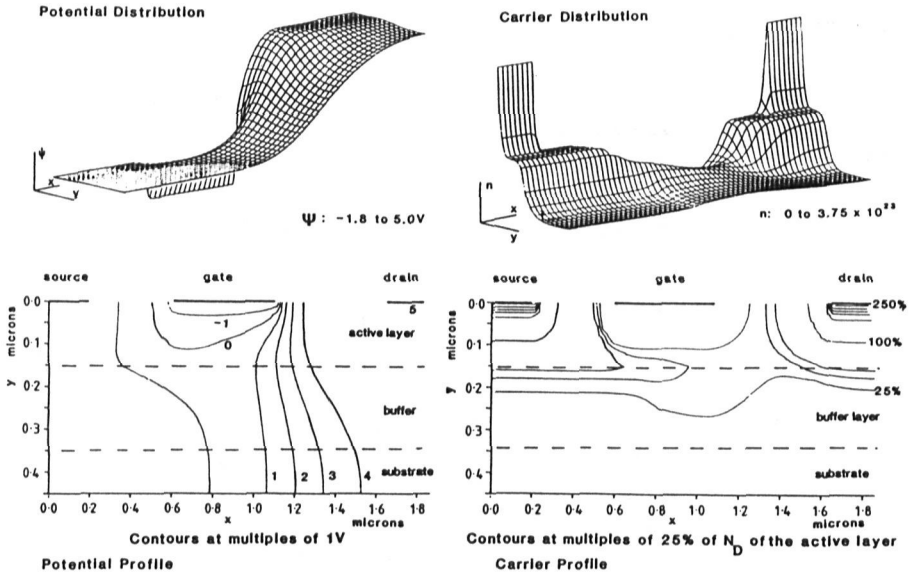


Figure 7  
 Potential and Carrier Distributions for  
 a  $0.5 \mu\text{m}$  gate-length MESFET with  $V_{DS}=5\text{v}$   $V_{GS}=-1\text{v}$

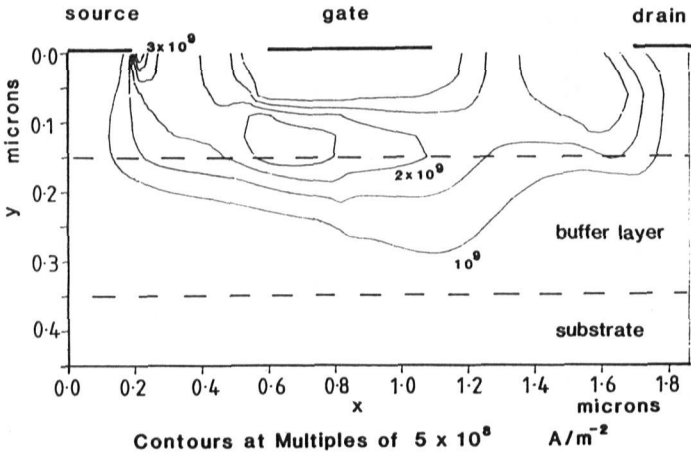


Figure 8  
 Distribution of the x component of current density

7. MMIC r.f. RESPONSES

An example of an MMIC oscillator which has been modelled using the MESFET simulation, in conjunction with a time domain circuit model, is shown in Figure 10. Typical examples of voltage and current responses obtained from this circuit are shown in Figure 11.

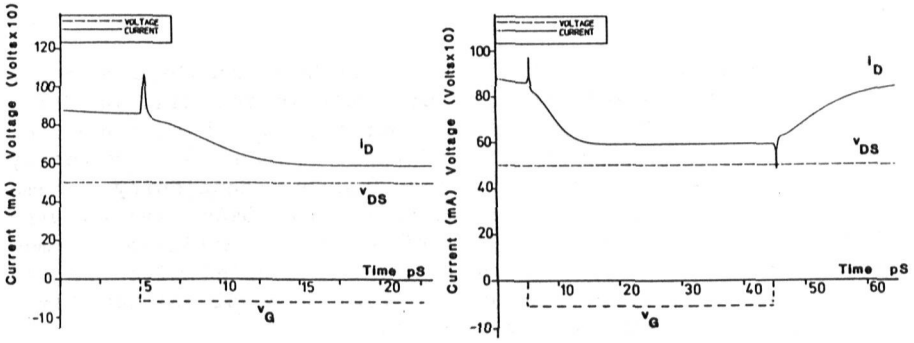


Figure 9  
Transient responses of the  $0.5 \mu\text{m}$  gate length MESFET

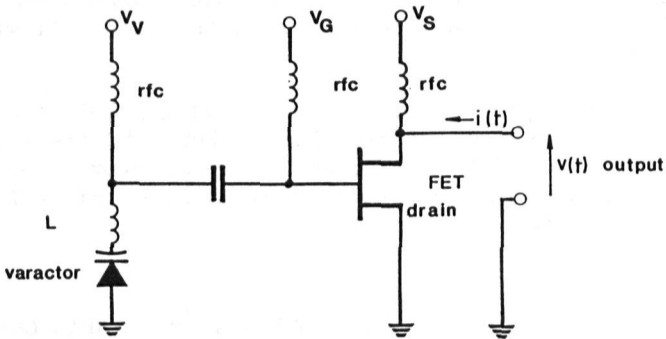


Figure 10  
Circuit Diagram of a MMIC Common Drain MESFET VCO

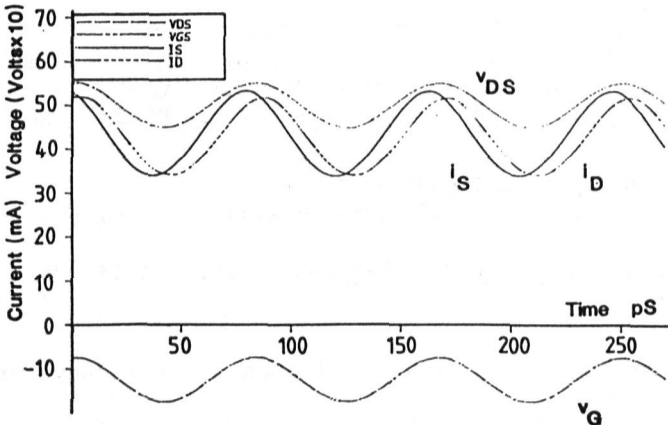


Figure 11  
Typical voltage and current responses of the circuit in Figure 10

CONCLUSIONS

The numerical simulation described here provides a means of accurately characterising short gate-length GaAs MESFETs. The use of a detailed electron-temperature model accounts for non-equilibrium transport conditions such as velocity overshoot. The specially developed current continuity scheme provides stable and accurate solutions for GaAs devices with high carrier densities in excess of  $10^{23}\text{m}^{-3}$ . Efficient formulation of the finite difference schemes, coupled with the use of a double-iteration technique, allows long simulation times in reasonable amounts of c.p.u. time.

The simulation has been applied to a  $0.5\ \mu\text{m}$  gate-length GaAs MESFET which has both the buffer layer and substrate included in the model. D.C. and transient characteristics of this FET have been predicted and found to agree well with measured devices.

Specific applications for this simulation lie in the design and analysis of simple MMICs, where the flexibility and accuracy of the model makes the technique attractive for CAD applications, and in the optimum design and characterisation of discrete devices.

REFERENCES

1. YOSHII, A., KITAZAWA, H., TOMIZAWA, M., HORIGUCHI, S. and SUDO, T.,  
"A Three-Dimensional Analysis of Semiconductor Devices"  
IEEE Trans. Electron Devices, Vol. ED-29, No.2, p.184  
1982.
2. HUSAIN, A. and CHAMBERLAIN, S.G.,  
"Three-Dimensional Simulation of VLSI MOSFET's: The  
Three-Dimensional Simulation Program WATMOS"  
IEEE Trans. Electron Devices, Vol. ED-29, No.4, p.631  
1982.
3. YAMAGUCHI, K. and KODERA, H.  
"Drain Conductance of Junction Gate FETs in the Hot Elec-  
tron Range"  
IEEE Trans. Electron Devices, Vol. ED-23, No.6, p.545  
1976.
4. REISER, M.,  
"Large-Scale Numerical Simulation in Semiconductor Device  
Modelling"  
Comp. Meth. Appl. Mech. Eng., Vol.1, p.17 1972.
5. KENNEDY, D.P. and O'BRIEN, R.R.,  
"Computer-Aided Two-Dimensional Analysis of the Junction  
Field-Effect Transistor"  
IBM J.Res. Develop., Vol.14, p.95 1970.

6. REISER, M.,  
"A Two-Dimensional Numerical FET Model for DC, AC, and Large-Signal Analysis"  
IEEE Trans. Electron Devices, Vol. ED-20, No.1, p.35 1973.
7. SNOWDEN, C.M., HOWES, M.J. and MORGAN, D.V.,  
"Large-Signal Modelling of GaAs MESFET Operation"  
IEEE Trans. Electron Devices, Vol. ED-30, No.12, p.1817 1983.
8. SNOWDEN, C.M., DOADES, G.P., HOWES, M.J., and MORGAN, D.V.,  
"Two Terminal Characterization of Microwave Monolithic Elements", In:Proc. 11th European Microwave Conference, Microwave Exhibitions and Publishers Ltd, Kent, England, p. 633 1981.
9. BLOTEKJAER, K.,  
"Transport Equations for Electrons in Two-Valley Semiconductors"  
IEEE Trans. Electron Devices Vol ED-17, No. 1, p. 38 1970.
10. CURTICE, W.R and YUN, Y-H,  
"A Temperature Model for the GaAs MESFET"  
IEEE Trans. Electron Devices, Vol. ED-28, No. 8, p. 954 1981.
11. CARROLL, J.E.,  
"Hot Electron Microwave Generators",  
Edward Arnold (Publishers), London, 1970.
12. FREEMAN, K.R. and HOBSON, G.S.,  
"The  $V_{fT}$  relation of CW Gunn Effect Devices"  
IEEE Trans. Electron Devices, Vol. ED-19, No. 1, p. 62 1972.
13. HILSUM, C.,  
"Simple Empirical Relationship Between Mobility and Carrier Concentration"  
Electronic Letters, Vol. 10., No. 12, p. 259 1974.
14. SZE, S.M.,  
"Physics of Semiconductor Devices",  
Wiley International, 1969.
15. GERALD, C.F.,  
"Applied Numerical Analysis"  
Adison and Wesley, London, 1973.
16. SHUR, H.S. and EASTMAN, L.F.,  
"Current-Voltage Characteristics, Small-signal Parameters and Switching Times of GaAs FETs"  
IEEE Trans. Electron Devices, Vol. ED-25, No. 6, p. 606 1978.